SINAI International Scientific Journal (SISJ)
Volume 2, Issue 1, July 2025

Investigating The Impact of Dynamic Characteristics on Surface Quality of Burnished AISI 1035 Steel Using Taguchi Analysis

Waleed F. Youssef [1], Mahmoud Elsamanty [2,3], M. Abdelsalam [4], A.A. Ibrahim [2]*

[1]Mechanical Engineering Department, Faculty of Engineering, Sinai University, Arish, North Sinai, Egypt.
[2]Mechanical Engineering Department, Faculty of Engineering at Shoubra, Benha University, Cairo, Egypt.
[3]Mechatronics and Robotics Department, School of Innovative Engineering Design, Egypt-Japan University of Science and Technology (E-JUST), Alexandria, Egypt.
[4]Department of Design and Production Engineering - Faculty of Engineering – Ain Shams University, Cairo, Egypt.
**Corresponding author*

Correspondence:

Waleed Farag Mohammed
Email: waleed.mohammed@su.edu.eg

Citation:

Youssef, W. F., Elsamanty, M., Abdelsalam, M., and Ibrahim, A. A. "Investigating The Impact of Dynamic Characteristics on Surface Quality of Burnished AISI 1035 Steel Using Taguchi Analysis", SINAI International Scientific Journal (SISJ), vol. 2, Issue 1, pp. 77-101, 2025.

Received: 29 July 2024

Accepted: 5 November 2024

ABSTRACT

The burnishing process is an important modern technology for producing mechanical parts with high-quality surface finishes. A special rigid burnishing tool was imported and used specially for the purpose of this research. Based on a Taguchi L16 matrix, an experimental test design was applied to study the effect of ball burnishing parameters as well as dynamic characteristics on the surface quality of burnished workpieces. The results of average surface roughness number, peaks counted per centimeter, out-of-roundness, and vibration amplitude were conducted. The workpieces burnished by the rigid tool retained a minimum surface roughness value of 0.107 µm at a burnishing speed of 500 RPM, 0.09 mm/rev feed rate, and 0.35 mm penetration depth. Regarding the out-of-roundness, the burnishing process using the imported rigid tool retained a minimum out-of-roundness value of 5.92 µm at a rotating speed of 600 RPM, a feed rate of 0.11 mm/rev, and a penetration depth of 0.35 mm. The increasing in vibration level achieved as the burnishing speed increases has a good effect on the surface roughness until the burnishing speed reaches a certain value. Beyond this speed value, the increase in vibration level induces the chatter phenomenon which badly affects the workpiece surface roughness. Regarding the out-of-roundness, the increasing in vibration level as the burnishing speed increases has a good impact on the roundness error of the burnished workpiece. These findings provide important insights for optimizing the metal burnishing process and achieving the desired surface quality based on the specific tool and associated factors.

KEYWORDS: Dynamic Characteristics, Vibration Amplitude, Surface Roughness, Out of Roundness, and Rigid Tool.

1. INTRODUCTION

Mechanical component performance is significantly influenced by surface characteristics [1]. The wear resistance, fatigue life, friction behavior, and corrosion resistance of a component are all strongly influenced by its surface finish [2]. A contemporary finishing method called burnishing enhances surface properties without removing any material from the workpiece [3, 4]. In cold working settings, this procedure includes pressing a hard tool into the workpiece's surface, generating plastic deformation beyond its yield stress [5]. Surface characteristics including hardness, corrosion resistance, and roughness can all be improved by burnishing [6]. Applying burnishing to the workpiece's surface and subsurface layers has been demonstrated in earlier studies to enhance surface hardness [7-9]. However, because of the

Online ISSN: 3009-7800
Print ISSN: 3009-6324

ball's slight deforming action at high speeds and high feed rates, burnishing speed increases cause a drop in surface hardness [10]. In a parallel manner, increasing burnishing feed reduces surface hardness, because a lower surface area is disposed to plastic deformation [11]. As a result of higher strain-hardening levels and higher work-hardening degrees brought about by deeper penetration, there is an increase in hardness. Higher penetration depth, however, raises the temperature of the workpiece and lowers surface hardness [12, 13]. Surface roughness is one of the characteristics that is most impacted by the burnishing process. Surface roughness falls to a minimum value when burnishing speed is increased, however, increases beyond that point result in surface roughness increasing once more [10]. Surface roughness is reduced as the feed rate increases because asperities plastically deform and there is higher surface contact between the tool and the workpiece. However, going over a certain point causes the surface profile to deteriorate and the micro-profile to become distorted [14]. Surface roughness is also affected by burnishing tool penetration, where a greater degree of plastic deformation results in a lower surface roughness [13, 15]. Out-of-roundness is an important surface feature to study when investigating burnished surfaces. Better out-of-roundness is achieved by increasing the burnishing speed; this is correlated with the increase in temperature at high burnishing speed levels in the ball-work interface. A higher temperature leads to material softening, which improves burnishing and reduces out-of-roundness mistakes [16]. On the other hand, increasing the burnishing feed rate causes a reduction in burnishing duration, which increases the out-of-roundness error [17]. While increasing the penetration depth increases the tool pressure on the workpiece surface, it first reduces the out-of-roundness mistake. However, because of over-hardening and the ensuing flaking of the surface layers, each additional increase in penetration depth gradually causes an increase in out-of-roundness error [18].

Without the need for costly and time-consuming tests, researchers can examine the effects of burnishing parameters on the stress distribution and plastic deformation in a workpiece's surface layer using the potent technique of finite element analysis (FEA) [19]. DEFORM-2D has been utilized extensively in finite element simulations. When using FEA in burnishing simulations, the best burnishing parameters such as feed, burnishing force, and speed can be found that produce the desired surface characteristics, like micro-hardness, residual stress, and surface roughness [16]. It is possible to accomplish the processes of burnishing and grinding simultaneously by installing the burnishing tool after applying the grinding process [20]. When ultrasonic burnishing is applied, advantageous compressive stresses and high surface quality are produced in components that require contact as a functional necessity [21]. The work surface's sliding burnishing design element characteristic is a feature that is fixed to the handle. ANSYS is utilized for burnishing parameters optimization. A three-dimensional finite element model is employed to predict the residual stresses generated by the process [22, 23]. The highest surface quality is attained when the depth of ball penetration into the workpiece material is almost equal to the maximum peak height [24, 25]. This is the best set of parameters for the LPB process, which is generated across the thickness of the component. A numerical simulation model for the CoTuB process is applied using a mixed technique and with a burnishing ball [26]. Furthermore, the 2024-T3 Al alloy may be effectively burnished using a single toroidal roller as a mixed burnishing process, and other process combinations can provide similar microstructures [27, 28]. In Ti-6Al-4V alloy, the hydraulic burnishing pressure is the most important factor in generating advantageous compressive residual stress with minimal cold work [29]. The hardness values of the materials

Online ISSN: 3009-7800
Print ISSN: 3009-6324

can be raised by a combined manufacturing process that maximizes harsh turning conditions, re-aging, and burnishing to improve surface quality and integrity [30, 31]. In addition, compared to the standard procedure, the energy consumption and roughness can be decreased by roughly 31.46% and 7.41%, respectively. The empirical data and the theoretical roughness values are slightly close [32, 33]. Ultimately, it is found that a higher burnishing effort increases the depth of the compressive zone while only marginally increasing the residual surface stresses [34]. A physic-based analytical model has conducted to investigate the hardening mechanism contributed to surface integrity enhancement during burnishing process. The concluded results showed that the there is a high contact between the measured and predicted values of hardness [35]. Even though earlier experimental findings offer some early understanding, comprehensive characterization across many controlled burnishing parameters is still required. The ability of burnishing to manage deviations from a desired geometric form, like out-of-roundness and surface roughness, is not well understood. It is becoming more and more crucial to quantify the way surface finishing procedures such as burnishing, produce very near-surface geometry, as manufacturing tolerances get tighter to meet the precision requirements of contemporary designs. Therefore, this research aims to quantify the influence of burnishing parameters on the process dynamics, as well as, the surface texture and roundness accuracy of AISI 1035 steel specimens.

2. MATERIALS AND METHODS

2.1. Workpiece Material

AISI 1035 steel is the workpiece material used in this study. It is a material that is frequently used in a variety of industrial applications. AISI 1035 steel is appropriate for the specified research goal because of certain features, such as high strength, good machinability, and a wide range of applications. It can be used in the manufacturing of power transmission shafts, gears, and power screws, this wide range of industrial applications is conducted on this type of steel also because of its ability to be heat and surface treated. Its 0.35 percent carbon content by weight places it in the medium carbon steel group. AISI 1035 steel's chemical composition is thoroughly broken down in Table 1, showing the specific amounts of each element present [36].

Table 1: Chemical Composition of AISI 1035 Steel [36].

Grade	Chemical Composition %				
	Fe%	**C%**	**Mn%**	**S%**	**P%**
C35	98.80	0.35	0.70	0.005	0.004

Table 2 [36] shows the mean values of AISI 1035 steel mechanical characteristics. Examples include density, tensile strength, yield strength, modulus of elasticity, bulk modulus, shear modulus, and thermal conductivity. These qualities reveal important information about the material's strength, toughness, and capacity to tolerate varying loading situations. To evaluate the workpiece's performance, a tension test was performed on a standard tension test specimen at a rate of loading 1 mm/min by the ASTM E8/E8M standard, as shown in Fig. 1, [37]. This test entails subjecting the specimen to steadily increasing tensile strains until it fails.

Online ISSN: 3009-7800
Print ISSN: 3009-6324

Fig. 2, depicts the stress-strain relationship and provides information about the material's deformation behavior, ultimate strength, and fracture characteristics.

Table 2: Mechanical Properties Analysis of AISI 1035 steel [36].

Grade	Density (g/cm^3)	Tensile Strength (MPa)	Yield Strength (MPa)	Modulus of Elasticity (GPa)	Bulk Modulus (GPa)	Shear Modulus (GPa)
C35	7.85	585	370	200	140	80

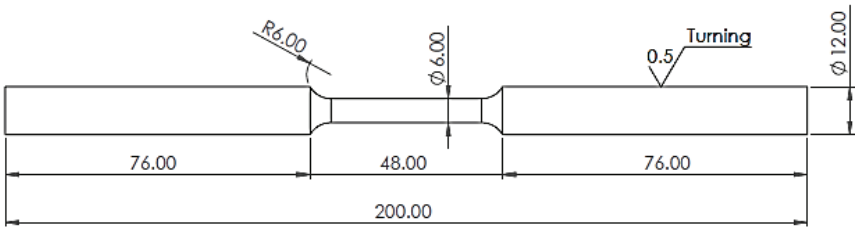

Fig. 1: Design of Tension Specimen According to ASTM E8/E8M [37].

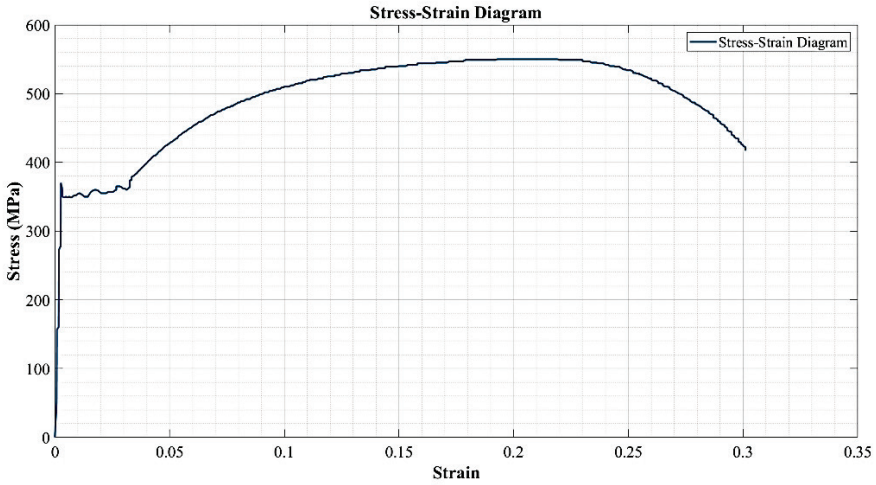

Fig. 2: Stress-Strain Diagram of AISI 1035 Steel from Tensile Test at Rate of Loading 1 mm/min.

The workpieces were made with a center lathe. Certain cutting parameters were used to produce the workpiece to the appropriate standards. These parameters included a rotational speed of 600 RPM, a cutting feed of 0.1 mm per revolution, and a cutting depth of 0.1 mm. These factors are critical for producing the appropriate surface finish, dimensional accuracy, and chip formation during machining. The workpiece was constructed to have a diameter of 50 mm and a length of 400 mm, with 10 test parts of 30 mm each, as illustrated in Fig. 3. Dimensions are crucial for ensuring that the workpiece is compatible with other components or systems with which it will be incorporated. The configuration shown in Fig. 3, is a data representation of the workpiece's general shape, including any special characteristics such as holes, or grooves.

Online ISSN: 3009-7800
Print ISSN: 3009-6324

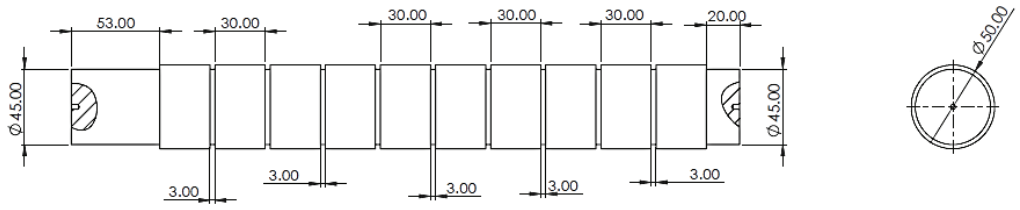

Fig. 3: Configuration of Burnishing Workpiece: A Detailed Representation of the Workpiece Design and Dimensions.

2.2. Burnishing Tool

Taizhou Ke Chi Machinery Company, a prominent Chinese manufacturer, produced a high-quality, precision-engineered stiff burnishing tool. This specific burnishing tool, indicated by the code JC-SQ8R2030, is intended to provide superior performance and accuracy in metal finishing tasks. The burnishing tool's 20x20 mm tool shank ensures outstanding stability and rigidity during machining. One unique feature of the burnishing tool is its 30-degree bent tip shape. This shape allows smooth and efficient burnishing operations, particularly in complex workpiece geometries or confined spaces. The bent tip increases maneuverability and gives precise control over the burnishing process, resulting in consistent and uniform surface finishes. The burnishing tool is loaded with an 8 mm tungsten carbide ball, noted for its high hardness and wear endurance. This material is known for its Young's modulus of 600 GPa with a maximum compression stress of 6000 MPa, these high values of mechanical properties have a good effect on the burnishing ball, leading it to withstand high force as well as friction stress generated from the contact between the ball and workpiece in the burnishing process. The 8 mm ball size provides optimal contact with the workpiece surface, enabling effective smoothing and refinement of imperfections. Fig. 4 depicts the burnishing tool, including its main components and specifications. The illustration shows the tool shank, the 30-degree bent tip, and the tungsten carbide ball. This visual reference provides a clear grasp of the tool's design, allowing for accurate identification and application in manufacturing. The main aim of purchasing the JC-SQ8R2030 burnishing tool from Taizhou Ke Chi Machinery Company is to improve the efficiency and precision of metal finishing operations. This tool's sturdy construction, bent tip design, and high-grade tungsten carbide ball allow for exceptional surface finishes, guaranteeing that the finished items match the required specifications and quality standards.

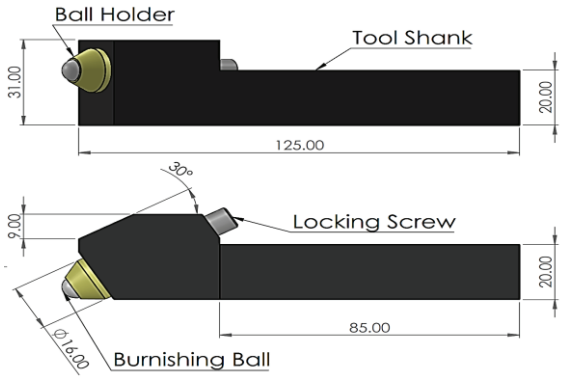

Fig. 4: A Schematic Representation of the Rigid Burnishing Tool Used in this Study.

Online ISSN: 3009-7800
Print ISSN: 3009-6324

This type of burnishing tool uses a rigid floating pressure device with a highly finished surface mounted on the tool shank to press the ball against the workpiece. The burnishing load transferred by this tool is high with a long-time ball life because of low friction between the tool and the floating pressure device. The products with surface finished by this tool shall have a high surface hardness with a noticeable wear resistance, the fatigue life of these products will also be improved. All these enhancements will extend the product life and positively affect the maintenance cost due to part replacement.

2.3. Testing Procedures and Measurements

The Taguchi experimental test design approach was used to study the influence of various parameters on the burnishing process. Each tool underwent 16 experiments utilizing the Taguchi method, resulting in a stable and efficient experimental design. The experimental components were chosen based on three quantitative variables: burnishing speed (N), feed rate (S), and tool depth of ball penetration ( ), each with four different values. Table 3 shows how the Taguchi Array was used to organize the specific levels and their matching combinations.

Table 3: Selected Burnishing Process Parameters Investigated for the Study.

Parameter	Burnishing Speed, $\boldsymbol{N}$ (RPM)	Burnishing Feed, $\boldsymbol{S}$ (mm/rev)	Depth of penetration, $\boldsymbol{h}$ (mm)
1	300	0.09	0.20
2	400	0.10	0.25
3	500	0.11	0.30
4	600	0.12	0.35

The arithmetic average roughness (R_a) and number of peaks counted per centimeter (R_{pc}) were used to assess surface roughness enhancement. As shown in Fig. 5, these parameters were measured with the Mitutoyo surftest SJ-201, a precision instrument designed specifically for surface roughness investigation. A cut-off length of 0.8 mm was chosen to ensure the measurements capture the critical surface features while minimizing the influence of longer wavelength fluctuations, this cutoff length is chosen from the measurement standard table based on some preliminary measurements. The workpiece was divided into five circumferential parts to ensure that all necessary data was collected to determine the best measurement locations, and also to reduce measurement error as possible as we can. Five readings were taken at each indicated place, and the arithmetic average of these five measured values was calculated.

Fig. 5: Setting Up of SJ-201 Mitutoyo Surftest to Measure the Surface Roughness for the Burnished Workpieces.

Online ISSN: 3009-7800
Print ISSN: 3009-6324

The specimens' out-of-roundness (O) was measured using a HEXAGON 257 coordinate measuring machine (CMM) with a sensitivity of 0.1 µm. One hundred points were measured around the circumference during the testing process. Fig. 6 depicts the measured out-of-roundness. The graphical representation shows the variances in the specimens' geometry, emphasizing any inconsistencies or deviations from the ideal round shape. The measurements taken by the HEXAGON 257 CMM machine provide useful insights into the specimens' out-of-roundness features, allowing for quantitative analysis and comparison of various experimental settings. The vibration analysis was performed using a 4514 B&K accelerometer and a B&K 2560 C Signal Analyzer, with the vibration signal measured in the time domain. The measured signal is saved as an Excel workbook for every experiment conducted in this study, the signal is digitalized by the analyzer and saved within four thousand points per signal. The vibration level (A) was determined by taking the root mean square of the saved signal points, this step is conducted manually using a programmed code in the Excel software. Fig. 7 shows the vibration measurement setup, including the accelerometer and the vibration analyzer setup. Fig. 8, displays the vibration signal measured in the time domain. Table 4 lists the experiments performed and the experimental data obtained for this investigation.

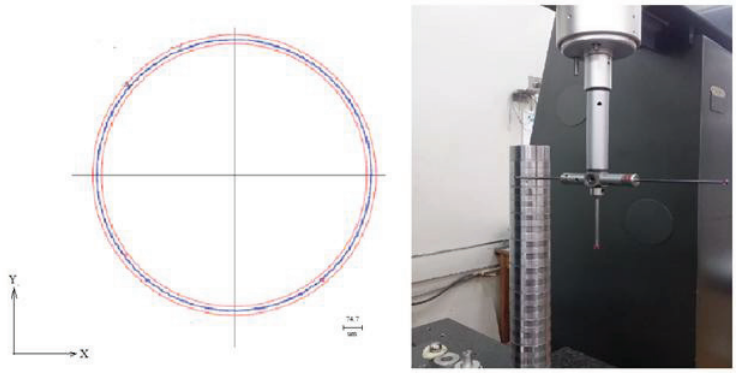

Fig. 6: Out-of-roundness measurements of the workpiece using a CMM machine.

Fig. 7: Setup of Vibration Measurement Equipment including, (a) the 4514 Accelerometer, and (b) the 2560 C Signal Analyzer.

Online ISSN: 3009-7800
Print ISSN: 3009-6324

Table 4: Taguchi L16 Experimental Design, and Investigation Outputs for Rigid Burnishing Tool.

No.	N (RPM)	S (mm/rev.)	h (mm)	Rigid Tool			
				R_a (µm)	R_{pc} (1/cm)	O (µm)	A (m/S²)
1	300	0.09	0.20	0.22	35.5	11	2.81
2	300	0.10	0.25	0.19	30	8.6	3.04
3	300	0.11	0.30	0.18	29.9	8.6	2.88
4	300	0.12	0.35	0.16	26.8	8.4	3.38
5	400	0.09	0.25	0.18	29.6	8.9	5.18
6	400	0.10	0.20	0.19	31	10.4	5.76
7	400	0.11	0.35	0.14	25.3	6.3	5.13
8	400	0.12	0.30	0.16	26.2	6.9	4.29
9	500	0.09	0.30	0.13	24	7.7	5.51
10	500	0.10	0.35	0.12	23.1	7.3	5.95
11	500	0.11	0.20	0.2	31.7	8.9	7.55
12	500	0.12	0.25	0.14	26.3	8	7.94
13	600	0.09	0.35	0.11	22.1	5.9	6.08
14	600	0.10	0.30	0.17	28.5	7.2	8.08
15	600	0.11	0.25	0.18	30	7.4	8.90
16	600	0.12	0.20	0.19	31.5	9.7	8.96

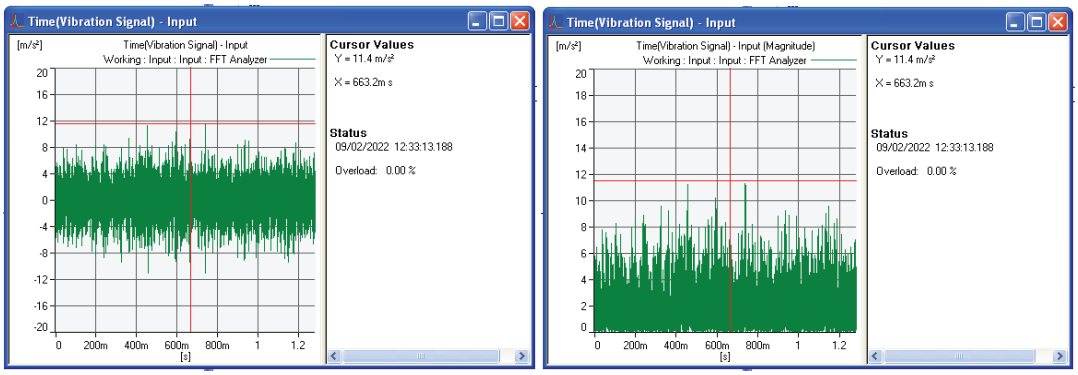

(a) **(b)**

Fig. 8: Online Vibration Signal Measured in The Time Domain including, (a) the working signal, and (b) the signal magnitude.

Online ISSN: 3009-7800
Print ISSN: 3009-6324

3. RESULTS AND DISCUSSIONS

3.1. Mathematical Modelling and Error Analysis

This work used Taguchi analysis to investigate the effect of burnishing parameters and dynamic characteristics, as well as to forecast the associated outcomes for reducing surface out-of-roundness and roughness. Following Taguchi's technique, loss functions were used to measure the difference between predicted and actual values. Low surface roughness and out-of-roundness are always preferable for improving product performance. Thus, the surface response parameters were classed as a "smaller is better" function. The signal-to-noise ratio (S/N ratio) was calculated using $\eta(R_a)$, $\eta(R_{pc})$, and $\eta(O)$ in this context. In terms of dynamic characteristics, the effect of vibration amplitude on surface parameters was unknown in this study, a "*nominal is better*" type function was employed to classify this parameter. The loss function definitions used in this study followed the "*lower is better*" criterion, while the "nominal is better" criterion was applied to n repeated measurements, denoted as y_i. The loss functions are expressed as follows:

$$LB_\eta = \left(\frac{S}{N}\right)_{LB} = -10\ log\ log\ \left[\frac{1}{n}\right]\sum_{i=1}^{n} \quad y_i^2 \tag{1}$$

$$NB_\eta = \left(\frac{S}{N}\right)_{NB} = 10\ log\ log\ \left[\frac{1}{n}\right]\sum_{i=1}^{n} \quad \frac{^2 - S_i^2}{S_i^2} \tag{2}$$

To establish the best ball burnishing process parameters, single response optimization was used to reduce surface roughness and out-of-roundness. The optimal effect of ball burnishing process parameters, such as rotating speed, burnishing feed, and penetration depth, was identified by plotting surface roughness and out-of-roundness main effect plots (MEP) with MINITAB 21 software. The signal-to-noise (S/N) ratio quality features of surface roughness factors and surface out-of-roundness were determined to evaluate the experimental outcomes, using the "the smaller, the better" method. Fig. 9, shows the main effect graphs for each response investigated in this study for the stiff tool. The Taguchi method was used to maximize the S/N ratio and determine the best cutting condition. Table 5 shows the optimal combination of input burnishing settings that produces the greatest outcomes for each response across the rigid burnishing tool. For example, the tool's minimal surface roughness may be reached at a burnishing speed of 500 rpm, a feed rate of 0.09 mm/rev, and a penetration depth of 0.35 mm. In terms of out-of-roundness, the rigid tool's minimal value was attained at a burnishing speed of 600 rpm, a feed rate of 0.11 mm/rev, and a penetration depth of 0.35mm. These optimum parameter combinations were determined using the Taguchi approach, resulting in superior burnishing results for the relevant responses.

Online ISSN: 3009-7800
Print ISSN: 3009-6324

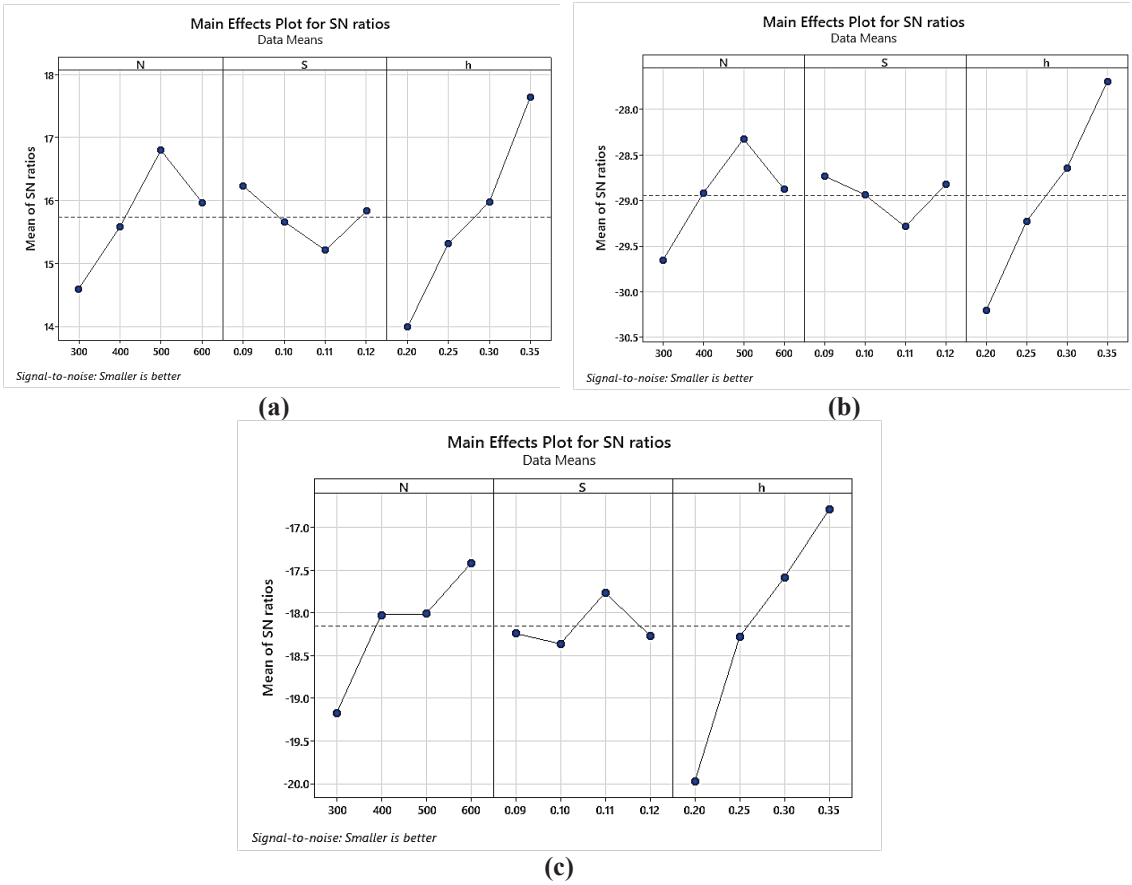

Fig. 9: Main effect Plot for S/N ratio of studied responses for rigid tool for, (a) R_a, (b) R_{pc}, and (c) O.

Table 5: Optimum ball burnishing parameters according to the Taguchi method for a rigid tool for R_a, R_{pc}, and O, respectively.

Responses	Rigid Tool		
	N	**S**	**H**
	RPM	**mm/rev**	**Mm**
$\boldsymbol{R_a}$	500	0.09	0.35
$\boldsymbol{R_{pc}}$	500	0.09	0.35
$\boldsymbol{O}$	600	0.11	0.35

The goal of this study was to determine the parameter values that resulted in the lowest surface roughness and out-of-roundness, hence increasing the product's overall performance. To accomplish this, the Taguchi approach was used to create mathematical models that define the relationship between burnishing response variables (surface roughness factors and out-of-roundness), as well as process dynamic characteristics and burnishing parameters for stiff burnishing tools. These models were created using Taguchi linear regression, followed by evaluation and analysis. During the evaluation phase, the ANOVA was used to determine the

Online ISSN: 3009-7800
Print ISSN: 3009-6324

significance of the process variables and their interactions. This statistical research shed light on the impact of burnishing factors on surface and dynamic features, enabling for more effective burnishing process optimization. Tables 6–21 describe the burnishing process modeling and analysis used in this study. The particular inspection and analysis of experimental data, as well as the mathematical models constructed using the Taguchi Method, allowed for a thorough knowledge of the link between burnishing response variables and burnishing parameters. This knowledge is an essential component for improving surface quality and overall product performance.

Table 6: Estimated Model Coefficients for R_a.

Term	Coef.	SE Coef.	*T*	*P*
Constant	0.166250	0.003461	48.034	0.000
N 300	0.021250	0.005995	3.545	0.012
N 400	0.001250	0.005995	0.209	0.842
N 500	-0.018750	0.005995	-3.128	0.020
S 0.09	-0.006250	0.005995	-1.043	0.337
S 0.10	0.001250	0.005995	0.209	0.842
S 0.11	0.008750	0.005995	1.460	0.195
h 0.20	0.033750	0.005995	5.630	0.001
h 0.25	0.006250	0.005995	1.043	0.337
h 0.30	-0.006250	0.005995	-1.043	0.337

Table 7: R_a Model Summary.

S	R-Sq	R-Sq(adj)
0.0138	92.00%	80.00%

Table 8: Analysis of Variance Table for R_a Model.

Source	DF	Seq SS	Adj SS	Adj MS	*F*	*P*
N	3	0.003275	0.003275	0.001092	5.70	0.034
S	3	0.000525	0.000525	0.000175	0.91	0.489
H	3	0.009425	0.009425	0.003142	16.39	0.003
Residual Error	6	0.001150	0.001150	0.000192		
Total	15	0.014375				

Online ISSN: 3009-7800
Print ISSN: 3009-6324

Table 9: Response Table for R_a Model.

Level	N	S	
1	0.1875	0.1600	0.2000
2	0.1675	0.1675	0.1725
3	0.1475	0.1750	0.1600
4	0.1625	0.1625	0.1325
Delta	0.0400	0.0150	0.0675
Rank	2	3	1

Table 10: Estimated Model Coefficients for R_{pc}.

Term	Coef.	SE Coef.	T	P
Constant	28.2188	0.3716	75.946	0.000
N 300	2.3312	0.6436	3.622	0.011
N 400	-0.1938	0.6436	-0.301	0.774
N 500	-1.9437	0.6436	-3.020	0.023
S 0.09	-0.4187	0.6436	-0.651	0.539
S 0.10	-0.0688	0.6436	-0.107	0.918
S 0.11	1.0063	0.6436	1.564	0.169
h 0.20	4.2062	0.6436	6.536	0.001
h 0.25	0.7562	0.6436	1.175	0.284
h 0.30	-1.0688	0.6436	-1.661	0.148

Table 11: R_{pc} Model Summary.

S	R-Sq	R-Sq(adj)
1.4863	93.19%	82.97%

Table 12: Analysis of Variance Table for R_{pc} Model.

Source	DF	Seq SS	Adj SS	Adj MS	F	P
N	3	37.152	37.152	12.384	5.61	0.036
S	3	5.847	5.847	1.949	0.88	0.501
	3	138.272	138.272	46.091	20.87	0.001
Residual Error	6	13.254	13.254	2.209		
Total	15	194.524				

Online ISSN: 3009-7800
Print ISSN: 3009-6324

Table 13: Response Table for R_{pc} Model.

Level	*N*	*S*	
1	30.55	27.80	32.42
2	28.03	28.15	28.98
3	26.27	29.23	27.15
4	28.02	27.70	24.33
Delta	4.28	1.53	8.10
Rank	2	3	1

Table 14: Estimated Model Coefficients for Out-of-Roundness.

Term	Coef.	SE Coef.	*T*	*P*
Constant	8.20000	0.1700	48.230	0.000
N 300	0.95000	0.2945	3.226	0.018
N 400	-0.07500	0.2945	-0.255	0.807
N 500	-0.22500	0.2945	-0.764	0.474
S 0.09	0.17500	0.2945	0.594	0.574
S 0.10	0.17500	0.2945	0.594	0.574
S 0.11	-0.40000	0.2945	-1.358	0.223
h 0.20	1.80000	0.2945	6.112	0.001
h 0.25	0.02500	0.2945	0.085	0.935
h 0.30	-0.60000	0.2945	-2.037	0.088

Table 15: Out-of-Roundness Model Summary.

S	R-Sq	R-Sq(adj)
0.6801	90.63%	76.56%

Table 16: Analysis of Variance for Out-of-Roundness Model.

Source	DF	Seq SS	Adj SS	Adj MS	F	P
N	3	5.5250	5.5250	1.8417	3.98	0.071
S	3	0.8950	0.8950	0.2983	0.65	0.614
H	3	20.4050	20.4050	6.8017	14.71	0.004
Residual Error	6	2.7750	2.7750	0.4625		
Total	15	29.6000				

Online ISSN: 3009-7800
Print ISSN: 3009-6324

Table 17: Response Table for Out-of-Roundness Model.

Level	N	S	H
1	9.150	8.375	10.000
2	8.125	8.375	8.225
3	7.975	7.800	7.600
4	7.550	8.250	6.975
Delta	1.600	0.575	3.025
Rank	2	3	1

Table 18: Estimated Model Coefficients for Vibration Amplitude.

Term	Coef.	SE Coef.	*T*	*P*
Constant	5.71593	0.1447	39.510	0.000
N 300	-2.68748	0.2506	-10.725	0.000
N 400	-0.62536	0.2506	-2.496	0.047
N 500	1.02194	0.2506	4.078	0.007
S 0.09	-0.82079	0.2506	-3.276	0.017
S 0.10	-0.00772	0.2506	-0.031	0.976
S 0.11	0.40267	0.2506	1.607	0.159
h 0.20	0.55387	0.2506	2.210	0.069
h 0.25	0.54993	0.2506	2.195	0.071
h 0.30	-0.52549	0.2506	-2.097	0.081

Table 19: Vibration Amplitude Model Summary.

S	R-Sq	R-Sq(adj)
0.5787	96.98%	92.46%

Table 20: Analysis of Variance for Vibration Amplitude Model.

Source	DF	Seq SS	Adj SS	Adj MS	*F*	*P*
N	3	55.625	55.625	18.5417	55.37	0.000
S	3	4.069	4.069	1.3563	4.05	0.068
	3	4.879	4.879	1.6264	4.86	0.048
Residual Error	6	2.009	2.009	0.3349		
Total	15	66.582				

Online ISSN: 3009-7800
Print ISSN: 3009-6324

Table 21: Response Table for Vibration Amplitude Model.

Level	N	S	
1	3.028	4.895	6.270
2	5.091	5.708	6.266
3	6.738	6.119	5.190
4	8.007	6.142	5.138
Delta	4.978	1.247	1.132
Rank	1	2	3

Predicting burnishing results by the experimental method used is a significant advantage of applying experimental test design procedures. Fig.10 (a) – (d), illustrates a comparison of experimental and expected findings using the Taguchi technique. Using the Taguchi experimental design approach, the experimental results of the surface quality indicators (R_a, R_{pc}, and O) as well as the vibration amplitude of the burnishing process of steel 50 bars by rigid tool used in this study are compared to the statistical values predicted. The figures show that there is little difference between the experimental and projected data, implying a little anticipated error between the various approaches. This shows that both strategies are effective at optimizing the burnishing operation and forecasting the burnishing results. The Taguchi technique determines the best prediction with the smallest feasible margin of error using percentage error analysis and mean percentage error. The expected error was calculated using the following formula:

$$Percentage\ Error\ (\%) = \left|\frac{Experimental\ Result - Predicted\ Result}{Experimental\ Result}\right| \times 100 \quad (3)$$

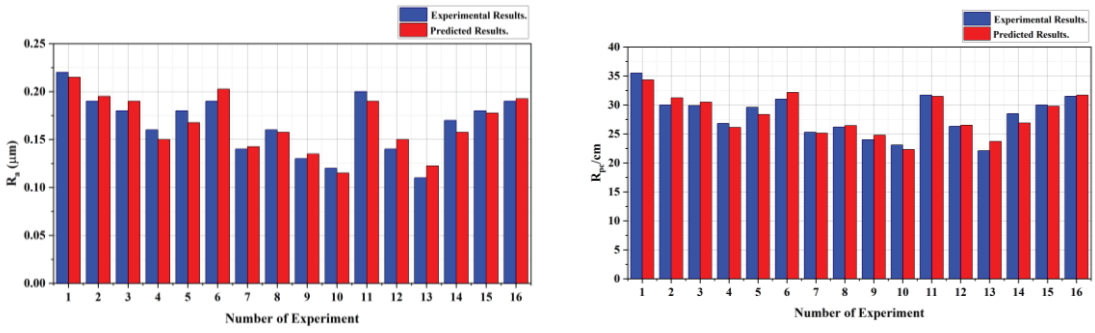

(a) **(b)**

Online ISSN: 3009-7800
Print ISSN: 3009-6324

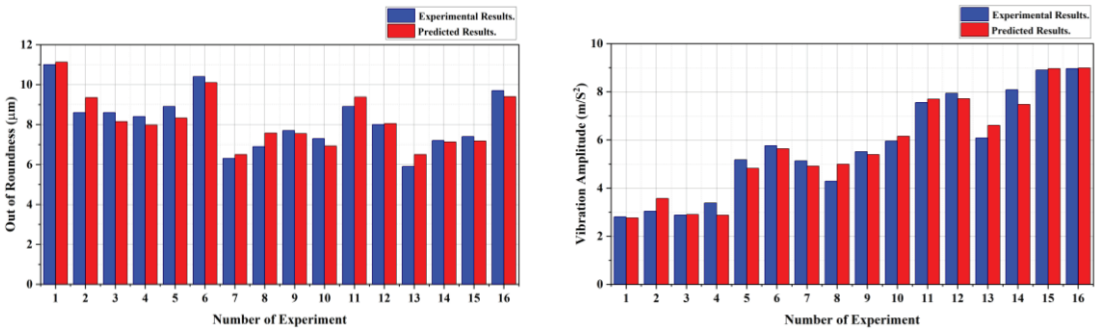

Fig. 10: Comparison Between Experimental and Taguchi Predicted Results for Surface Characteristics of Workpiece Burnished by Rigid Tool for (a) R_a, (b) R_{pc}, (c) O, and (d) A.

Fig. 11, depicts an error analysis for surface and dynamic properties using a rigid burnishing tool. The chart shows that, at all design sites, the Taguchi technique's percentage error for surface characteristics is minor, not exceeding 11.36%. In some design points, the Taguchi technique predicts a much larger mistake in vibration amplitude than the surface characteristics error. The Taguchi technique produces a maximum inaccuracy of 17.44%. Fig. 12 compares the mean percentage errors for the surface and dynamic properties of the burnishing process using the Taguchi method. The Taguchi technique calculates a maximum anticipated error of 5.76%. This tiny result shows that the Taguchi approach is appropriate and effective for industrial applications.

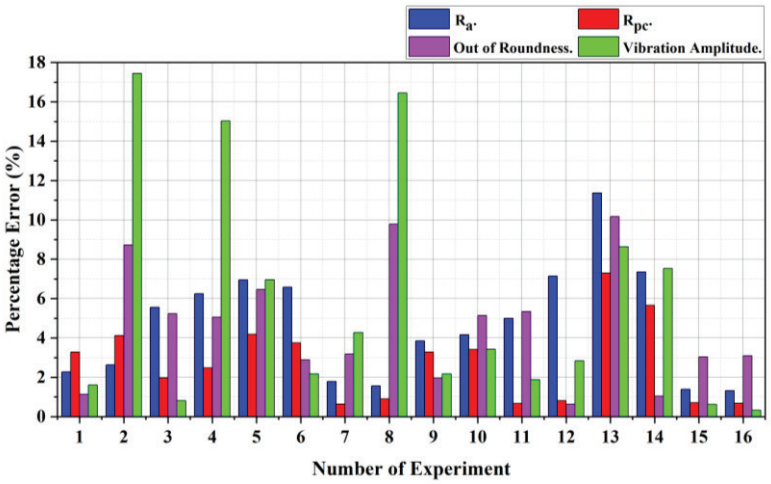

Fig. 11: Comparison Between Percentage Error of Taguchi Method of Surface Characteristics for Workpiece Burnished by Rigid Burnishing Tool.

Online ISSN: 3009-7800
Print ISSN: 3009-6324

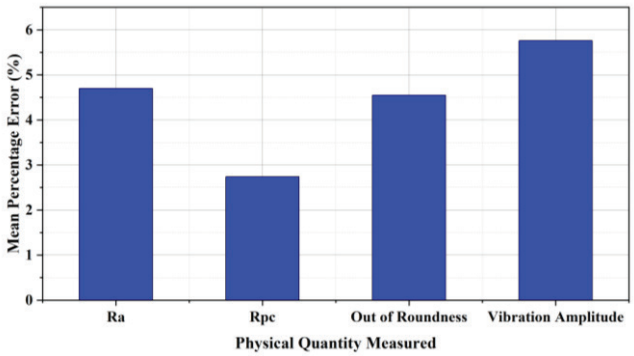

Fig. 12: Mean Percentage Error of Taguchi Method of Surface Characteristics for Workpiece Burnished by Rigid Burnishing Tool.

3.2. Effect of Burnishing Parameters on Surface and Dynamic Characteristics of AISI 1035 Steel

3.2.1. Burnishing Speed

Fig. 13 (a) depicts the relationship between burnishing speed and the surface roughness arithmetic average (R_a) of a workpiece burnished with a rigid tool. The graph offers vital information on the impact of burnishing speed variation on surface roughness. For all depth of penetration values, as burnishing speed increases, surface roughness decreases until it reaches its minimum value at 500 RPM. This reduction in surface roughness can be attributed to the increased material flow and refinement caused by the higher burnishing speed. However, surpassing the ideal speed threshold may result in increased surface roughness caused by chatter, an undesired vibration-induced phenomenon [38,39]. The enhancement in surface roughness due to the change in burnishing speed with the optimum feed rate and depth of penetration is 27 % as calculated from the data. Fig. 13 (b) shows the relationship between burnishing speed and the number of peaks per centimeter (R_{pc}) on a workpiece that was polished using a rigid tool. The graph depicts the impact of burnishing speed on surface peaks. Initially, as the burnishing speed increases, the surface peaks decrease, reaching a minimum of 500 RPM for all penetration levels. The lower surface peaks can be attributed to increased material flow and refinement generated by the faster burnishing pace. However, exceeding the ideal speed threshold might result in greater surface peaks due to chatter, which causes unwanted vibrations and flaws on the workpiece surface [38,39]. The chatter generated by vibration causes unwanted ball traces to be formed on the workpiece surface, resulting in higher peaks counted. The reduction in surface peaks counted due to the change in burnishing speed with the optimum feed rate and depth of penetration is 16.4 % as calculated from the data. Fig. 13 (c) depicts the relationship between burnishing speed and out-of-roundness (O) of the workpiece burnished with the rigid tool. Burnishing speed reduces surface out-of-roundness, reaching a minimum value at a maximum speed of 600 RPM, as per the research interval for all penetration values. This pattern can be traced in part to the fact that the burnishing ball's deforming effect is less pronounced at low speeds and becomes more noticeable as speed increases. However, according to prior research, increased burnishing speed result in a large increase in roundness inaccuracy [38,39]. The enhancement in out-of-roundness due to the change in burnishing speed with the optimum feed rate and depth of penetration is 21.83 % as calculated from the data. Fig. 13 (d) depicts the relationship between burnishing speed and

Online ISSN: 3009-7800
Print ISSN: 3009-6324

vibration amplitude of the workpiece subjected to burnishing using the rigid tool. The graph shows that increasing the burnishing speed at any penetration value leads to an increase in vibration amplitude until it reaches its maximum value of 8.98 m/s2 at a maximum speed of 600 RPM with a feed rate of 0.12 mm/rev and 0.2 mm depth of penetration according to the study interval. This phenomenon can be attributed to the increase in negative damping as the burnishing ball rolls on the workpiece surface while the burnishing speed increases [40].

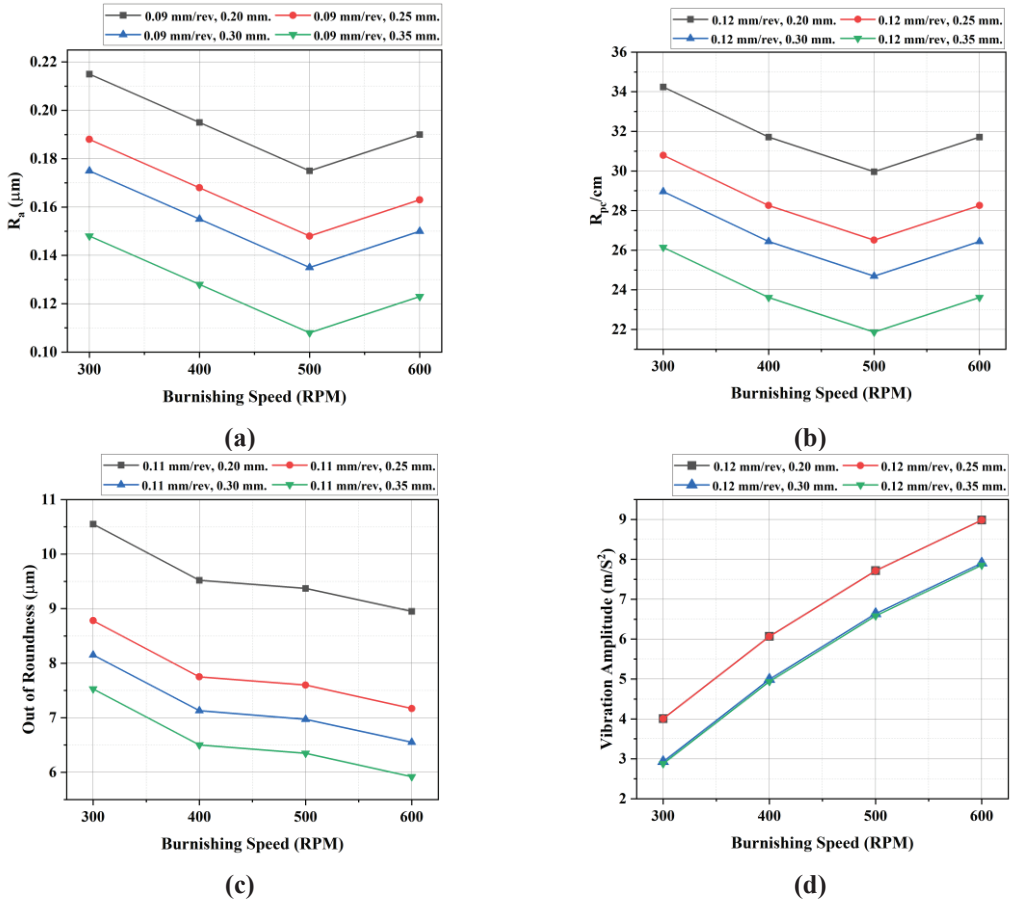

Fig. 13: Effect of Burnishing Speed on the Surface Characteristics of Workpiece Burnished by Rigid Tool for (a) R_a, (b) R_{pc}, (c) O, and (d) A.

3.2.2 Burnishing Feed Rate

Fig. 14 (a) demonstrates the relationship between feed rate and average surface roughness while employing a rigid tool. However, earlier research has shown that as the feed rate increased, the surface roughness decreased until it reached an optimum value, at which point it began to increase again [38,39]. This analysis revealed a unique tendency. Notably, when the feed rate is increased, the workpiece's surface finish increases until it reaches its maximum value of 0.163 µm when the feed rate reaches a value of 0.11 mm/rev with a speed of 300 RPM and depth of penetration of 0.35 mm, then the trend is reversed. The change in the area of contact between the ball and the workpiece is considered the main reason for such an effect.

Online ISSN: 3009-7800
Print ISSN: 3009-6324

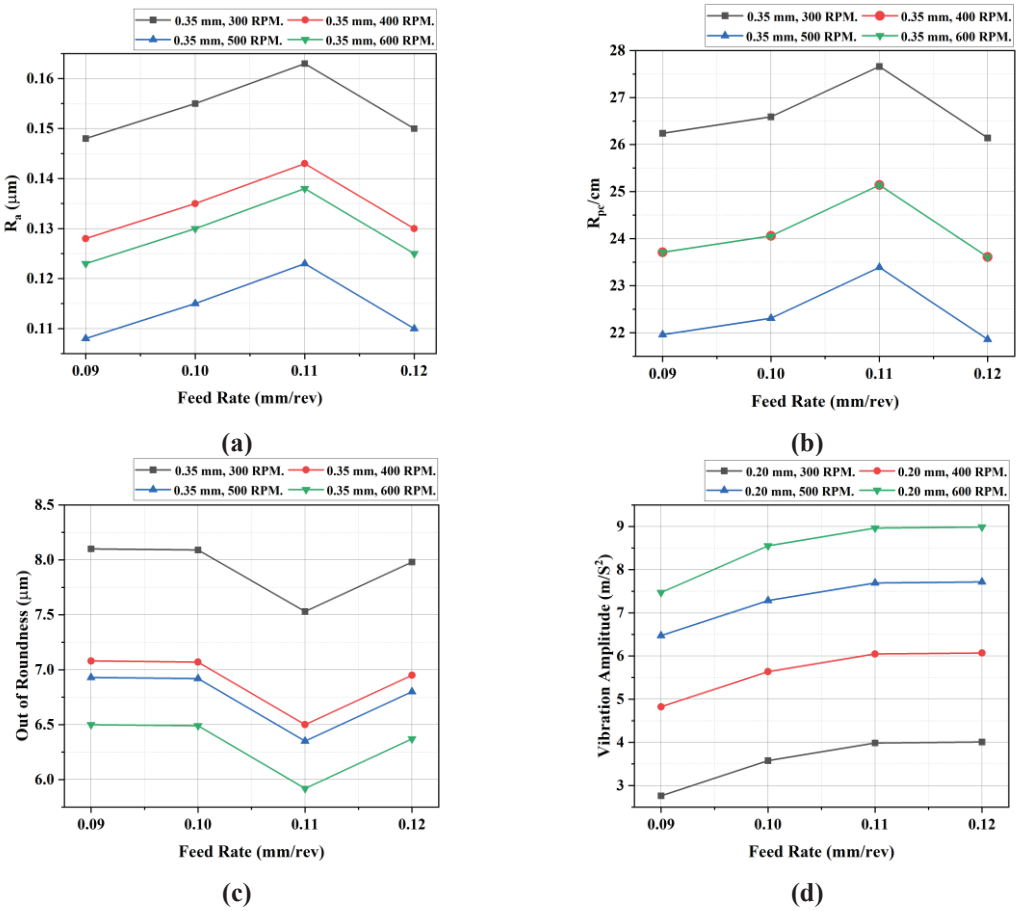

Fig. 14: Effect of Feed Rate on the Surface Characteristics of Workpiece Burnished by Rigid Tool for (a) R_a, (b) R_{pc}, (c) O, and (d) A.

Fig. 14 (b) demonstrates the relationship between feed rate and number of peak counts while using a rigid tool. A previous study found that increasing the feed rate reduced surface roughness until it reached an optimum, after which it increased again [38, 39]. This investigation revealed a different pattern. Notably, raising the feed rate causes the workpiece's peaks to rise to reach its maximum value of 27.66/cm at a feed rate of 0.11 mm/rev, after which it is dropped again. The alteration in the region of contact between the ball and the workpiece is regarded to be the primary component causing such an impact. Unwanted ball traces are formed on the workpiece surface due to the difference in contact area, resulting in high number of peaks counted. Fig. 14 (c) depicts the relationship between burnishing feed rate and roundness error when a rigid tool is used. The burnished surface's out-of-roundness decreases with increasing feed rate at any burnishing speed value, reaching a minimum value at 0.11 mm/rev then the roundness error started to increase again according to the research interval. This phenomenon could be explained by changes in the contact area between the burnishing ball and the workpiece, as well as the tool's bend angle. Changed contact circumstances affect material flow and deformation, minimizing surface imperfections and out-of-roundness. Previous research has shown the same effect [38,39]. The enhancement in out-of-roundness due to the change in burnishing feed rate with the optimum speed and depth of penetration is 8.92 % as calculated from the data. Fig. 14 (d) depicts the relationship between the burnishing

Online ISSN: 3009-7800
Print ISSN: 3009-6324

feed rate and vibration amplitude of the workpiece subjected to burnishing using the rigid tool. The graph shows that increasing the burnishing feed leads to an increase in vibration amplitude until it reaches its maximum value of 8.98 m/s2 at a maximum feed rate of 0.12 mm/rev with a speed of 600 RPM and 0.2 mm depth of penetration according to the study interval. The increasing in negative damping due to rolling of the burnishing ball on the workpiece surface as the feed rate increases is the main reason of this phenomenon [40].

3.2.3. Depth of Penetration

Fig. 15 (a) depicts the connection between average surface roughness and depth of penetration when a rigid tool is applied. Surface roughness decreases with penetration depth for any feed value, reaching its minimum value at 0.35 mm.

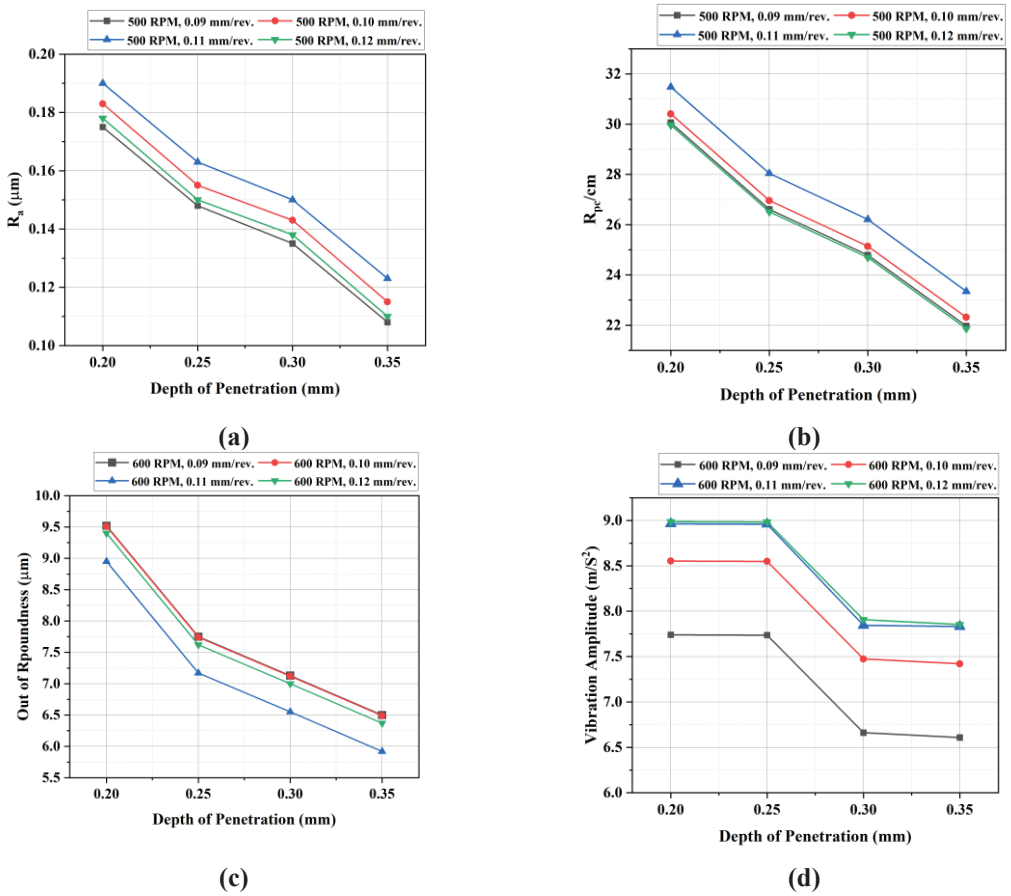

Fig. 15: Effect of Depth of Penetration on the Surface Characteristics of Workpiece Burnished by Rigid Tool for (a) R_a, (b) R_{pc}, (c) O, and (d) A.

This trend can be explained by increased penetration depths resulting in more pronounced plastic deformation, leading to smoother surfaces. Increased plastic deformation improves material flow and rearrangement, leading to better surface burnishing. Otherwise, prior research found that increasing the depth of penetration reduced surface roughness until a specific value was reached, after which further increasing penetration increased surface roughness [38,39]. The enhancement in surface roughness due to the change in burnishing depth of penetration with the optimum feed rate and burnishing speed is 38.29 % as calculated

Online ISSN: 3009-7800
Print ISSN: 3009-6324

from the data. Fig. 15 (b) illustrates the relationship between surface peak count and depth of penetration when a rigid tool is used. The findings show that increasing penetration depth reduces surface peaks until they approach a minimum value of 0.35 mm for any feed rate across the study interval. Higher penetration depths cause more intense plastic deformation, resulting in smoother surfaces. Increased plastic deformation promotes material flow and rearrangement, resulting in a smoother surface. Alternatively, earlier research revealed that increasing the depth of penetration reduced surface roughness until a particular value was achieved, after which further increasing penetration increased surface roughness [38,39]. The reduction in surface peaks counted due to the change in burnishing depth of penetration with the optimum feed rate and burnishing speed is 27 % as calculated from the data. Fig. 15 (c) depicts the relationship between the depth of penetration and the out-of-roundness (O) of a workpiece burnished with a rigid tool for any feed rate value. The surface's out-of-roundness decreases with penetration depth, reaching a minimum value of 0.35 mm. This can be due to the increased ball pressure and hence higher plastic deformation, which contribute to a more uniform and more round surface profile. Previous research found that when the depth of penetration increased, the out-of-roundness also decreased [38,39]. The enhancement in out-of-roundness due to the change in depth of penetration with the optimum feed rate and burnishing speed is 33.85 % as calculated from the data. Fig. 15 (d) depicts the relationship between burnishing depth of penetration and vibration amplitude of the workpiece subjected to burnishing using the rigid tool. The graph shows that increasing the penetration value at any feed rate leads to a decrease in vibration amplitude until it reaches its minimum value of 6.6 m/s2 at a maximum depth of penetration of 0.35 mm with a speed of 600 RPM and feed rate of 0.09 mm/rev according to the study interval. The increasing penetration of the ball into the workpiece causes an increase in positive damping, this increase in damping makes the vibration amplitude to be decreased as known leading to this phenomenon [40].

3.3. Relationship Vibration Amplitude and Surface Characteristics of Burnished AISI 1035 Steel

Fig. 16 (a) displays the relationship between the vibration amplitude and the surface roughness arithmetic average (Ra) when the burnishing speed is the varying parameter for a workpiece burnished using the rigid tool. The graph indicates as the burnishing speed increased the increasing vibration amplitude reduced the surface roughness until it reached a minimum value of 0.107 µm at a speed of 500 RPM, 0.09 mm/rev feed rate, and 0.35 mm depth of penetration, as per the research interval. Any further increase in the vibration amplitude caused by the increase in burnishing speed value enhances the chatter to be induced causing an increase in surface roughness. Fig.16 (b) shows the relationship between vibration amplitude and out-of-roundness (O) when burnishing speed is a variable parameter for a workpiece burnished with a rigid tool. The graph indicates that increasing burnishing speed reduces out-of-roundness to a minimum of 5.92 µm at 600 RPM, 0.11 mm/rev feed rate, and 0.35 mm depth of penetration, according to the research interval. In this case, the vibration level has a favorable effect on the roundness of the workpiece.

Online ISSN: 3009-7800
Print ISSN: 3009-6324

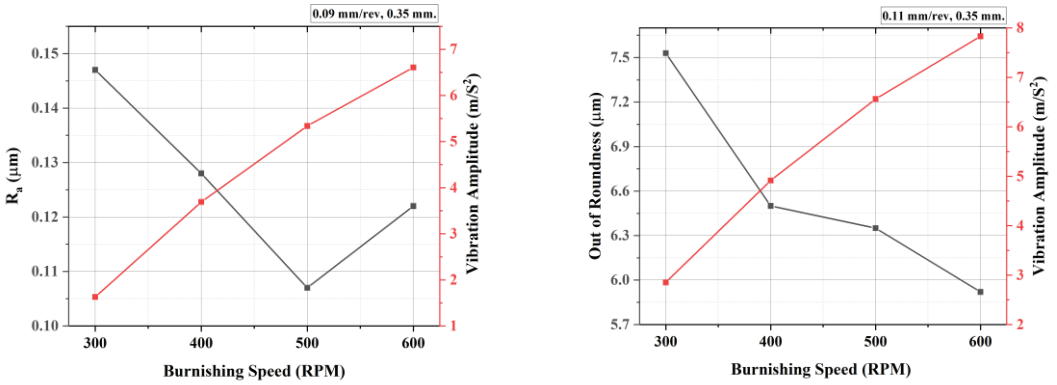

(a) (b)

Fig. 16: Effect of Variation of Vibration Amplitude with the Burnishing Speed on the Workpiece Burnished by the Rigid Tool for (a) Surface Roughness, (b) Out-of-Roundness.

4. CONCLUSIONS

This study conducted a thorough assessment of the effect of process parameters as well as dynamic characteristics on surface roughness and out-of-roundness in the burnishing process. A series of studies were carried out using a delivered rigid burnishing tool and a Taguchi L16 matrix was applied to evaluate the effects of burnishing parameters on the workpiece surface characteristics. The results of this study show that the relationship between burnishing parameters and surface roughness, as well as out-of-roundness, is determined and compared with the vibration level induced during the burnishing process. Notably, optimal parameter combinations were identified for each surface characteristic as follows:

- The minimum surface roughness achieved by this study using the rigid burnishing tool is 0.107 µm at a rotational speed of 500 RPM, feed rate of 0.09 mm/rev, and penetration depth of 0.35 mm.
- The minimum out-of-roundness value attained by the burnishing process using the imported rigid tool is 5.92 µm at a rotating speed of 600 RPM, feed rate of 0.11 mm/rev, and penetration depth of 0.35 mm.
- The increasing vibration level achieved as the burnishing speed increased has a good effect on the surface roughness until the burnishing speed reaches a value of 500 RPM, according to the research interval.
- Beyond the optimum speed value, the increase in vibration level induces the chatter phenomenon which has a bad effect on the surface roughness.
- Regarding the out-of-roundness, the increasing vibration level as the burnishing speed increased has a good effect on the roundness error of the burnished workpiece, according to the research interval.

These findings provide important insights for optimizing the metal burnishing process and achieving the desired surface quality based on the specific tool and associated factors.

Online ISSN: 3009-7800
Print ISSN: 3009-6324

CONFLICT OF INTEREST

No conflict of interest.

FUNDING

None is declared

REFERENCES

[1] Prasad K, John M. Optimization of external roller burnishing process on magnesium silicon carbide metal matrix composite using response surface methodology. Journal of the Brazilian Society of Mechanical Sciences and Engineering. 2021; 43(7):1–12.

[2] Rotella G, Caruso S, Antonio Del Prete, Filice L. Prediction of Surface Integrity Parameters in Roller Burnishing of Ti6Al4V. Metals. 2020; 10(12):1–17.

[3] El-Taweel T, El-Axir M. Analysis and optimization of the ball burnishing process through the Taguchi technique. The international journal of advanced manufacturing technology/International journal, advanced manufacturing technology. 2008; 41(3-4):301–310.

[4] Dave K, Panara R, Del Vadiya P. Design and Development of Ball Burnishing Tool. International Journal of Creative Research Thoughts. 2017; 6:733–738.

[5] Shetty S, Pavan Kumar K. Analysis on effect of ball burnishing processes of EN24 Steel. International Journal of Advance Research. 2018; 4(3):1262–1268.

[6] Loriya S, Patel V. A Review Paper on Ball Burnishing Process to Predict Surface Finish and Surface Hardness. International Journal of Engineering Research & Technology. 2018; 7(2):172–175.

[7] Mahato D, Verma A. Roller Burnishing - A Literature Review of Developments and Trends in Approach to Industrial Application. Asian Journal of Engineering and Technology. 2017; 1(3):68–83.

[8] Ismail N, Khatif N, Kecik M, Shaharudin M. The effect of heat treatment on the hardness and impact properties of medium carbon steel. IOP Conference Series: Materials Science and Engineering. 2016; 114:012108.

[9] Nasir N, Daud M, Selamat M, Rivai A, Malingam S. The Effect of Heat Treatment on Fatigue and Mechanical Properties of 6061 Aluminium Alloy. Applied Mechanics and Materials. 2014; 699:227–32.

[10] Fattouh M, El-Axir M, Serage S. Investigations into the burnishing of external cylindrical surfaces of Cu-Zn alloy. Wear. 1988; 127(2):123–37.

[11] Sachin B, Narendranath S, Chakradhar D. Effect of working parameters on the surface integrity in cryogenic diamond burnishing of 17-4 PH stainless steel with a novel diamond burnishing tool. Journal of Manufacturing Processes. 2019; 38(5):64–71.

[12] Nguyen T, Le M. Optimization of the Internal Roller Burnishing Process for Energy Reduction and Surface Properties. Journal of Mechanical Engineering. 2021; 67(4):167–179.

[13] Nguyen T, Cao L, Dang X, Nguyen T, Trinh Q. Multi-objective optimization of the flat burnishing process for energy efficiency and surface characteristics. Materials and Manufacturing Processes. 2019; 34(16):1888–1901.

[14] Kurkute V, Chavan ST. Modeling and Optimization of surface roughness and microhardness for roller burnishing process using response surface methodology for Aluminum 63400 alloy. Procedia Manufacturing. 2018; 20:542–547.

Online ISSN: 3009-7800
Print ISSN: 3009-6324

[15] John M, Vinayagam B. Optimization of nonlinear characteristics of ball burnishing process using Sugeno fuzzy neural system. Journal of the Brazilian Society of Mechanical Sciences and Engineering. 2013; 36(1):101–109.
[16] John M, Wilson A, Bhardwaj A, Abraham A, and Vinayagam B. An investigation of ball burnishing process on CNC lathe using finite element analysis. Simulation modelling practice and theory. 2016; 62:88–101.
[17] Boozarpoor M, Elyasi M, Hosseinzadeh M. An investigation of the surface quality of burnished AISI 4340 steel. Journal of Process Mechanical Engineering. 2017; 232(3):299–313.
[18] El-Axir M, Othman O, and Abodiena A. Improvements in out-of-roundness and microhardness of inner surfaces by internal ball burnishing process. Journal of materials processing technology. 2008; 196(1-3):120–128.
[19] Grochała D, Berczyński S, Zenon Grządziel. Modeling of burnishing thermally toughened X42CrMo4 steel with a ceramic ZrO 2 ball. Archives of Civil and Mechanical Engineering. 2017; 17(4):1011–1018.
[20] Charfeddine Y, Youssef S, Sghaier S, Hamdi H. Finite Element Residual Stress Computation for Combined Grinding/Burnishing Applied to 100Cr6 Steel. Lecture Notes in Mechanical Engineering. 2020; 131–137.
[21] Ullah R, Fangnon E, Juha Huuki. Effect of Ultrasonic Burnishing Parameters on Burnished-Surface Quality of Stainless Steel After Heat Treatment. Lecture notes in mechanical engineering. 2022; 38–47.
[22] Yadav P, Ghatge D. Analysis of Optimized Roller Burnishing Parameters Using ANSYS. Lecture notes on multidisciplinary industrial engineering. 2018; 55–61.
[23] Sayahi M, Sghaier S, and Belhadjsalah H. Finite element analysis of ball burnishing process: comparisons between numerical results and experiments. The International Journal of Advanced Manufacturing Technology. 2012; 67(5-8):1665–1673.
[24] Mohammadi F, Sedaghati R, Bonakdar A. Finite element analysis and design optimization of low plasticity burnishing process. The International Journal of Advanced Manufacturing Technology. 2013; 70(5-8):1337–1354.
[25] Randjelovic S, Tadic B, Todorovic P, Vukelic D, Miloradovic D, Radenkovic M, et al. Modelling of the ball burnishing process with a high-stiffness tool. The International Journal of Advanced Manufacturing Technology. 2015; 81(9-12):1509–1518.
[26] Rami A, Kallel A, Djemaa S, Mabrouki T, Sghaier S, Hamdi H. Numerical assessment of residual stresses induced by combining turning-burnishing (CoTuB) process of AISI 4140 steel using 3D simulation based on a mixed approach. The International Journal of Advanced Manufacturing Technology. 2018; 97(5-8):1897–1912.
[27] Duncheva G, Maximov J, Dunchev V, Anchev A, Atanasov T, Capek J. Single toroidal roller burnishing of 2024-T3 Al alloy implemented as mixed burnishing process. The International Journal of Advanced Manufacturing Technology. 2020; 111(11-12):3559–3570.
[28] Rotella G, Saffioti M, Sanguedolce M, Umbrello D. Finite element modelling of combined turning/burnishing effects on surface integrity of Ti6Al4V alloy. The International Journal of Advanced Manufacturing Technology. 2021; 119(1-2):177–187.

Online ISSN: 3009-7800
Print ISSN: 3009-6324

[29] Harish N, Shivalingappa D, Raghavendra N. The Impact of Low Plasticity Burnishing Process Parameters on Residual Stress and Percentage of Cold Working Distribution in Ti-6Al-4V Alloy. Journal of Failure Analysis and Prevention. 2021; 21(2):410–418.
[30] Rami A, Gharbi F, Sghaier S, Hamdi H. Some insights on Combined Turning-Burnishing (CoTuB) process on workpiece surface integrity. International Journal of Precision Engineering and Manufacturing. 2018; 19(1):67–78.
[31] Sönmez F, Başak H, Güral A, Baday Ş. Investigating the Efficiency of Secondary Aging and Burnishing Process in Friction Stir Welded Al-7075-T6 Material. International Journal of Precision Engineering and Manufacturing. 2018; 19(10):1515–1520.
[32] Nguyen T, Cao L. Optimization of the Burnishing Process for Energy Responses and Surface Properties. International Journal of Precision Engineering and Manufacturing. 2020; 21(6):1143–1152.
[33] Felhő C, Varga G. CAD and FEM Modelling of Theoretical Roughness in Diamond Burnishing. International Journal of Precision Engineering and Manufacturing. 2022; 23(4):375–384
[34] Duncheva G, Maximov J, Anchev A, Dunchev V, Atanasov T, Capek J. Finite element and experimental study of the residual stresses in 2024-T3 Al alloy treated via single toroidal roller burnishing. Journal of the Brazilian Society of Mechanical Sciences and Engineering. 2021; 43(1).
[35] Skoczypiec S, Teimouri R, Grabowski M, Bogucki R, and Łukasz S. Modeling of strengthening mechanisms of surface layers in burnishing process. Materials & Design. 2022; 223:111–126.
[36] Daniyan I, Mpofu K, Adeodu A, and Azeez T. Investigating the Quality and Conformity of Carbon Steel AISI 1035 under Varying Heat Treatment Conditions. Procedia Manufacturing. 2019; 35:1111–1116.
[37] ASTM Standards. Standard Test Methods for Tension Testing of Metallic Materials 1. 2013.
[38] Ibrahim A. An investigation into ball burnishing process of carbon steel on a lathe. Al-Azhar engineering 10th international conference. 2008; 1–12.
[39] El-axir M. and Ibrahim A. Some surface characteristics due to center rest ball burnishing. Journal of materials processing technology. 2005; 167(1):47–53.
[40] Hirose M, Hayasaka T, Shamoto E. Unique regenerative chatter in wiper-turning operation with burnishing process: Part 2: Experimental verification of predicted generation mechanism, critical stability, and characteristics. Precision Engineering. 2020; 71:304–312.

Online ISSN: 3009-7800
Print ISSN: 3009-6324